A new family of reduced models for non-isothermal falling films

Nicolas Cellier, Christian Ruyer-Quil

A new family of reduced models for non-isothermal falling films.

Nicolas Cellier[a], Christian Ruyer-Quil[a]

[a] *LOCIE, UMR 5271, CNRS, Universite Savoie Mont Blanc, Le Bourget-du-Lac, France*

Abstract

New asymptotic models are formulated to capture the thermal transfer across falling films. These models enable to simulate a wide range of Biot and Peclet number values, without displaying nonphysical behaviors. The models correctly capture the onset of the thermally developed regime at the inlet of the flow. To evaluate the parameter space of acceptability, a comparison has been made with the primitive equation solution for periodic boundary conditions, as well as for an open flow with a periodic forcing at inlet. A good agreement is obtained for moderate to high Peclet numbers.

Keywords: heat transfer, falling films, asymptotic expansion

Introduction

Falling films form thin layers of liquid flowing on a tilted plate, with a thickness of the order of a millimeter or less. Starting with the works of Nusselt [17], followed by Kapitza and Kapitza [12], this topic has been heavily studied and the hydrodynamic of a tilted falling film flowing on a smooth plate is well known. Curiously, the interplay between heat or mass transfers and the wavy dynamics of a falling films has been far less studied, even though Frisk and Davis [7], Yoshimura et al. [24] demonstrated that the wavy regime of the film can indeed increase several folds the heat and mass transfer coefficients between the liquid and the gas. Most studies on heat and mass transfer across the film focus on the wave-less smooth film situation [13]. Only a few studies have been devoted to the wavy regime and addressed heat transfer and hydrodynamics couplings by solving the Fourier equation across the film, the hydrodynamics being dealt with the

Email addresses: contact@nicolas-cellier.net (Nicolas Cellier), christan.ruyer-quil@univ-smb.fr (Christian Ruyer-Quil)

Navier-Stokes equations or a reduced model. The former approach leads to expensive computations, hardly compatible with a parametric study of the phenomena. It has been restricted either to 2D simulations in a domain corresponding to a full exchanger plate [22], or to numerical domains of limited extensions [9, 8, 23, 16, 15]. The latter approach allows better performances with acceptable accuracy, but is still not fast enough to allow extensive studies, such as sensibility analyses or optimizations. This explains a lack a numerical studies of non-isothermal falling films, the computation being too expensive to simulate evolution on a full exchanger plate for a significant time interval at a reasonable cost.

Another approach is to use reduced models for both fluid dynamic and heat transfer as proposed by Hirshburg and Florschuetz [10] some years ago, but under a fully-linear assumption for the temperature field. The convection effect has thus been neglected. Later, Ruyer-Quil et al. [20] have developed a reduced model, based on the weighted residual integrated boundary layer (WRIBL) approach. They considered a linear distribution of the temperature field as a closure hypothesis. This linear distribution was parameterized with only one variable corresponding to the free surface temperature $\theta = T|_{\bar{y}=1}$. Unfortunately, this model shows nonphysical behaviors at large Peclet numbers, as the temperature field may lie outside the admissible range. More recently, Chhay et al. [5] derived a one-equation model in a conservative and Galilean-transform invariant form. In that case, the temperature is bounded, but the model introduced a non-physical critical value $\theta_c = 7/22$ at which convective terms cancel out. It seems that a more complex parametrization of the temperature field is required to overcome this deficiency.

A cure to these shortcomings have been proposed with a two fields parametrization (Cellier [4]), adding a second variable $\phi = \partial_y T\, h|_{\bar{y}=0}$ corresponding to the heat flux at the wall. This approach leads to better results than before, but still shows some nonphysical behaviors, with an unbounded temperature. Moreover, the relaxation terms were not correctly accounted for, non-stationary simulations showing a faster development of the wall thermal boundary layer in the case of the primitive Fourier equation than predicted by the model. While not being an issue when studying fully developed traveling waves, it impedes the simulation of heat transfer whenever the thermal healing length is not negligible compared to the exchanger dimension. This is especially the case when the

Peclet number is increased.

In this study, we propose a new non-isothermal falling film model in which the temperature field is parameterized with two variables:

$$\theta = T|_{\bar{y}=1} \qquad \varphi = h^2 \frac{\partial^2 T}{\partial y^2}\Big|_{\bar{y}=1} . \tag{1}$$

This is an attempt to overcome the limitation of the modeling proposed by Ruyer-Quil et al. [20] and Chhay et al. [5] by adding more accuracy in the temperature field representation, and obtain a model that possesses coherent relaxation factors.

The paper is structured as follows: section 1 presents the problem to be solved. Our modeling attempt follows in section 2. We next discuss time-dependent simulations of heat transfer across falling liquid films in extended domains using our model (section 3).

1. Primitive equations

Notations

We consider a plane making an angle β with the horizontal. We restrict ourselves to the two-dimensional case where the solution is independent of the span-wise coordinate, and we introduce x and y to refer to the steam-wise and cross-stream coordinates respectively. A film of thickness h flows on a plane maintained at a constant temperature T_w and exchanges heat with a cold atmosphere T_a with a constant heat transfer coefficient H.

Here we turn directly to dimensionless equations and choose a scaling based on the Nusselt film thickness $h_N = [3\nu q_L/(g\sin\beta)]^{1/3}$ and the velocity $3u_N = g\sin\beta h_N^2/\nu$ corresponding to three times the averaged velocity of the Nusselt solution, where q_L is the volumetric flow rate per unit span-wise length, $\nu = \mu/\rho$ is the kinematic viscosity and g is the gravitational acceleration. Our choice of a velocity scale corresponds to the speed of kinematic waves generated by the deformation of the free surface in the long-wave limit, as traveling waves have a speed close to it.

The dimensionless primitive equations thus consist in the Navier-Stokes equations

$$3\mathrm{Re}\,(\partial_t u + u\partial_x u + v\partial_y u) = -\partial_x p + \partial_{xx} u + \partial_{yy} u + 1\,, \tag{2a}$$

$$3\mathrm{Re}\,(\partial_t v + u\partial_x v + v\partial_y v) = -\partial_y p + \partial_{xx} v + \partial_{yy} v\,, \tag{2b}$$

$$\partial_x u + \partial_y v = 0\,, \tag{2c}$$

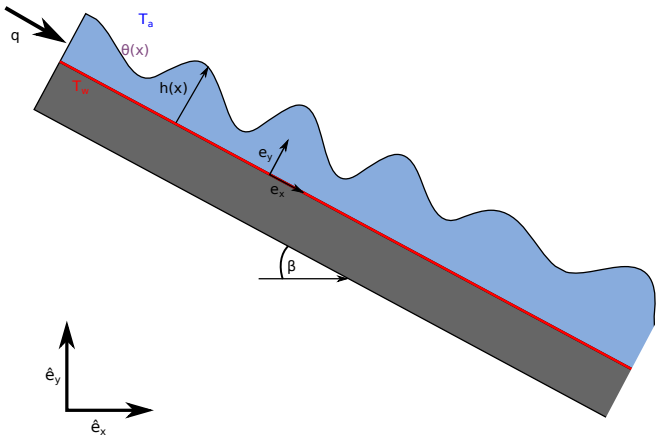

Figure 1: Sketch of a heated falling film (slice).

the Fourier equation

$$3\,\mathrm{Pr}\,\mathrm{Re}\,(\partial_t T + u\partial_x T + v\partial_y T) = \partial_{xx} T + \partial_{yy} T\,, \tag{2d}$$

completed by the no-slip condition at the wall

$$u = v = 0 \qquad \text{at} \quad y = 0\,, \tag{2e}$$

the kinematic condition at the free surface

$$\partial_t h + u|_h \partial_x h = v|_h\,, \tag{2f}$$

a temperature imposed condition at the wall and a Newton law of cooling at the free surface

$$T = 1 \qquad \text{at} \qquad y = 0\,, \tag{2g}$$

$$\partial_y T - \partial_x h \partial_x T = -\mathrm{Bi} T\sqrt{1 + (\partial_x h)^2} \qquad \text{at} \qquad y = h\,. \tag{2h}$$

We note that equation 2f is formally equivalent to the mass balance

$$\partial_t h + \partial_x q = 0 \tag{2i}$$

where $q = \int_0^h u dy$ is the flow rate. $\mathrm{Re} = \frac{u_N\, h_N}{\nu} = \frac{q_L}{\nu}$ is the Reynolds number and $\mathrm{Pr} = \frac{\nu}{\alpha}$ is the Prandtl number. Finally, $\mathrm{Bi} = \frac{H\, h_N}{k}$ is the Biot number, where α, k and H are the thermal diffusivity, the conductivity and the convective heat transfer coefficient.

2. Development

In the following, we focus on the derivation of averaged heat equations which enables us to solve the heat transfer within the film more easily than solving the Fourier equation (2d) within the framework of the long-wave assumption. We thus introduce a film parameter ε as the ratio of the typical thickness of the film to the typical length of the waves. The derivatives are of the order of this ε term, with respect to the stream-wise direction x or with time, as the film evolution is assumed to be slow. As a consequence, the cross-stream velocity is $v = -\int_0^y \partial_x u dy = O(\varepsilon)$.

Within this framework, we further assume that the velocity field u remains close to the parabolic profile corresponding to the Nusselt flow, i.e.

$$u = u^{(0)} + O(\varepsilon) \tag{3}$$

$$= \frac{3q}{h}\left(\bar{y} - \frac{1}{2}\bar{y}^2\right) + O(\varepsilon)\,, \tag{4}$$

where $q = \int_0^h u\, dy$ is the local flow rate and $\bar{y} = y/h$ is a reduced coordinate. The velocity field is thus parameterized with two variables, the film thickness h and the local flow rate q, whose evolution is governed by the mass balance (2i) and an averaged momentum balance. Several models have been proposed within this framework. Let us cite for instance, the model proposed by Vila and coworkers [1].

We thus aim at an integral approximation of the energy balance which mimics the elimination of the cross-stream coordinate that is achieved in Saint-Venant like models. To this aim, we shall project the temperature distribution onto a cleverly chosen set of functions. The associated amplitudes of these functions will form our parametrization of the temperature field. The evolution equations associated to these amplitudes will approximate the variations in space and time of the temperature within the waves. Let us first consider that the temperature distribution is never too far from its stationary ($\partial_t = 0$) and uniform ($\partial_x = 0$) distribution, i.e. a linear distribution given by:

$$T_{\mathrm{Nu}} = 1 + \left(\frac{1}{1 + \mathrm{Bi}h} - 1\right)\bar{y}\,. \tag{5}$$

In the very long-wave assumption ($\partial_x = 0$) and considering that the film thickness h and velocity field (u, v) are known (and constant), linearization of the energy balance around

the conductive equilibrium $T = T_{\rm Nu} + \tilde{T}$, $\tilde{T} \ll T_{\rm Nu}$ leads to

$$3{\rm Re}\,{\rm Pr}\,h^2\partial_t\tilde{T} = \partial_{\bar{y}\bar{y}}\tilde{T} \equiv \mathcal{L}\tilde{T} \quad \text{with} \quad \tilde{T}|_{\bar{y}=0} = 0 \quad \text{and} \quad \partial_{\bar{y}}\tilde{T}|_1 + {\rm Bi}h\tilde{T}|_1 = 0 \tag{6}$$

where again $\bar{y} = y/h$. The discrete spectrum of the diffusion operator $\mathcal{L} = \partial_{yy}$, eigenfunctions $v_n(\bar{y})$ and eigenvalues λ_n are given by

$$v_n = \sin(l_n\,\bar{y}), \quad \lambda_n = -\frac{l_n^2}{3\,{\rm Pr}\,{\rm Re}} \tag{7a}$$

where l_n are solutions to

$$l\cot l + {\rm Bi}h = 0\,. \tag{7b}$$

All eigenvalues λ_n are real and negative. They correspond to relaxation modes promoted by the diffusion of heat across the film.

Two limits are worth investigating. The first one is ${\rm Bi} = 0$ which corresponds to an insulated free surface, in which case the $T_{\rm Nu} = 1$ is constant and equal to its value at the wall. The second limit is ${\rm Bi} \to \infty$, in which case the free surface is at the constant temperature $T = 0$ (equal to the temperature of the gas phase).

For ${\rm Bi} = 0$,the discrete spectrum of $\mathcal{L}$ is

$$l_1 = \frac{\pi}{2}\,, \qquad l_2 = \frac{3\pi}{2}\,, \qquad l_3 = \frac{5\pi}{2}\,, \tag{8a}$$

$$3\,{\rm Pr}\,{\rm Re}\lambda_1 \approx -2.47\,, \qquad 3\,{\rm Pr}\,{\rm Re}\lambda_2 \approx -22.21\,, \qquad 3\,{\rm Pr}\,{\rm Re}\lambda_3 \approx -61.69\,. \tag{8b}$$

For ${\rm Bi} \to \infty$ we have instead

$$l_1 = \pi\,, \qquad l_2 = 2\pi\,, \qquad l_3 = 3\pi\,, \tag{9a}$$

$$3\,{\rm Pr}\,{\rm Re}\lambda_1 \approx -9.87\,, \qquad 3\,{\rm Pr}\,{\rm Re}\lambda_2 \approx -39.48\,, \qquad 3\,{\rm Pr}\,{\rm Re}\lambda_3 \approx -88.83\,. \tag{9b}$$

Following Roberts [18], we shall assume that the time evolution of the temperature is determined by the evolution on a manifold that is tangent to the first eigenmodes (7). It is clear that only a few eigenmodes should play a role as the eigenvalues rapidly become low and the corresponding relaxation times are shorter and shorter.

Let us thus decompose the temperature field into

$$T = T_{\rm Nu} + T^{(0)} + T^{(1)}\,, \tag{10}$$

where $T^{(0)}$ is aligned with the two first eigenmodes v_1 and v_2. Because l_1 and l_2 are not given explicitly but indirectly through the solution to (7b), it is more convenient to use polynomial approximations.

Requiring that $\tilde{v}_1(\bar{y})$ verifies

$$\tilde{v}_1'(1) + \mathrm{Bi}h\tilde{v}_1(1) = 0\,, \qquad \tilde{v}_1(0) = 0\,, \tag{11a}$$

$$\text{for} \quad \mathrm{Bi}h = 0\,, \qquad \tilde{v}_1(1) = 1\,, \qquad \tilde{v}_1'(1) = 0\,, \tag{11b}$$

$$\text{for} \quad \mathrm{Bi}h = \infty\,, \qquad \tilde{v}_1(1) = 0\,, \qquad \tilde{v}_1'(1) = 1\,, \tag{11c}$$

and that

$$\tilde{v}_2'(1) + \mathrm{Bi}h\tilde{v}_2(1) = 0\,, \qquad \tilde{v}_2(0) = 0\,, \tag{12a}$$

$$\text{for} \quad \mathrm{Bi}h = 0\,, \qquad \tilde{v}_2(1) = 1\,, \qquad \tilde{v}_2'(1) = 0\,, \qquad \tilde{v}_2(2/3) = 0\,, \tag{12b}$$

$$\text{for} \quad \mathrm{Bi}h = \infty\,, \qquad \tilde{v}_2(1) = 0\,, \qquad \tilde{v}_2'(1) = 1\,, \qquad \tilde{v}_2(1/2) = 0\,, \tag{12c}$$

which gives

$$\tilde{v}_1 = \bar{y}(2-\bar{y}) + \mathrm{Bi}h\,\bar{y}(1-\bar{y})\,, \tag{13}$$

$$\tilde{v}_2 = -12\bar{y}\left(\frac{2}{3}-\bar{y}\right)\left(\frac{5}{4}-\bar{y}\right) + \mathrm{Bi}h\,2\bar{y}(1-\bar{y})\left(\bar{y}-\frac{1}{2}\right)\,. \tag{14}$$

$\tilde{v}_1$ and $\tilde{v}_2$ are polynomial approximations to the relaxation eigenmodes v_1 and v_2. We introduce a linear combination of $\tilde{v}_1$, $\tilde{v}_2$ and two variables to represent the departure of the temperature field from the linear temperature distribution. The choice of these variables is particularly important. In order to fully capture the onset of a thermal boundary layer close to the stagnation point at the front of the waves, we chose variables which monitor the temperature distribution close to the free surface. The simplest choice is thus to use the free-surface temperature $\theta = T(y = h)$ as a variable.

We first introduce the ansatz

$$T^{(0)} = [\theta - \theta_0(h)]\hat{v}_1(\bar{y}) \qquad \text{with} \qquad \theta_0 = \frac{1}{1+\mathrm{Bi}h} \tag{15}$$

where

$$\hat{v}_1 = \bar{y}[3 - 3\bar{y} + \bar{y}^2 + \mathrm{Bi}h(2 - 3\bar{y} + \bar{y}^2)] \tag{16}$$

is a linear combination of $\tilde{v}_1$ and $\tilde{v}_2$ which verifies $\hat{v}_1'(0) = 0$ and $\hat{v}_1(1) = 1$. According to our choice of variables, the decomposition (10) with (15) is set unique by the gauge

condition

$$T^{(1)}|_{y=h} = 0\,. \tag{17}$$

Inserting the decomposition (10), (15) in (2d) gives

$$\partial_{yy}T^{(1)} = 3\,\mathrm{Pr}\,\mathrm{Re}\,(\partial_t + u\partial_x + v\partial_y)\,(T_{\mathrm{Nu}} + T^{(0)}) - \partial_{xx}(T_{\mathrm{Nu}} + T^{(0)})\,. \tag{18a}$$

Here, the second-order corrections to the advection terms $3\,\mathrm{Pr}\,\mathrm{Re}\,(\partial_t + u\partial_x + v\partial_y)\,T^{(1)}$ have been dropped out while the diffusion terms have been retained. This is justified considering that (i) these corrections are small compared to the other advection terms, (ii) all leading-order physical contributions have been retained in (18a). We note that solving (18a) is similar to looking for $T^{(1)}$ in terms of an expansion $T^{(1)} = \varepsilon T_1^{(1)} + \varepsilon^2 T_2^{(1)} + \ldots$ with respect to the film parameter where only the leading-order contributions are retained. Equation (18a) is completed with the boundary conditions

$$T^{(1)} = 0 \quad \text{at} \quad y = 0\,, \tag{18b}$$

$$\partial_y T^{(1)} = \partial_x h\partial_x(T_{\mathrm{Nu}} + T^{(0)}) - \mathrm{Bi}(T_{\mathrm{Nu}} + T^{(0)})(1 + \frac{1}{2}(\partial_x h)^2) \quad \text{at} \quad y = h\,. \tag{18c}$$

Solving (18) gives the correction $T^{(1)}$ as a polynomial in y whose coefficients are dependent on the variables h, q, θ, φ and their derivatives. The gauge condition (17) then provides an evolution equation for the variables θ, namely

$$\begin{aligned} 3\,\mathrm{Pr}\,\mathrm{Re}\partial_t\theta = {} & 3\,\mathrm{Pr}\,\mathrm{Re}\left\{-\frac{3(82+\mathrm{Bi}h)}{7(27+7\mathrm{Bi}h)}\frac{q}{h}\partial_x\theta - \frac{57\mathrm{Bi}}{7(27+7\mathrm{Bi}h)}\frac{q\theta}{h}\partial_x h\right. \\ & \left.+\frac{3[11+(-11+38\mathrm{Bi}h)\theta]}{14(27+7\mathrm{Bi}h)}\partial_x q\right\} - \frac{60(1+\mathrm{Bi}h)}{27+7\mathrm{Bi}h}\frac{\theta-\theta^{(0)}}{h^2} \\ & +\partial_{xx}\theta + \left(\frac{6+3(-2+7\mathrm{Bi}h)\theta}{27+7\mathrm{Bi}h}\right)\frac{\partial_{xx}h}{h} + \left(\frac{6+6(-1+2\mathrm{Bi}h)\theta}{27+7\mathrm{Bi}h}\right)\frac{(\partial_x h)^2}{h^2} \\ & +\left(\frac{6(8+7\mathrm{Bi}h)\theta}{27+7\mathrm{Bi}h}\right)\frac{\partial_x h\partial_x\theta}{h}\,, \end{aligned} \tag{19}$$

referred hereinafter as the θ model.

In essence, equation (19) is an averaged energy balance which must be compared to the model derived by Ruyer-Quil et al. [20] using the method of weighted residuals:

$$\begin{aligned} 3\,\mathrm{Pr}\,\mathrm{Re}\partial_t\theta = {} & 3\,\mathrm{Pr}\,\mathrm{Re}\left\{-\frac{27}{20}\frac{q}{h}\partial_x\theta + \frac{7}{40}\frac{(1-\theta)}{h}\partial_x q\right\} - 3\frac{\theta-\theta^{(0)}}{h^2} \\ & +\partial_{xx}\theta + (1-\theta)\frac{\partial_{xx}h}{h} + \left(1-\theta-\frac{3}{2}\mathrm{Bi}h\right)\frac{(\partial_x h)^2}{h^2} + \frac{\partial_x h\partial_x\theta}{h} \end{aligned} \tag{20}$$

The two energy balances are consistent with the long-wave expansion up to first-order for the convection terms and second-order for the diffusion terms. However, (19) represents a significant improvement over the former formulation (20). Figure 2a compares the relaxation coefficient

$$\lambda_\theta = -\frac{60(1+\mathrm{Bi}h)}{27+7\mathrm{Bi}h} \tag{21}$$

to the eigenvalue λ_1. As expected, a much better agreement is observed with the new formulation (19).

A first validation of the modeling approach is offered by the construction of the traveling-wave solutions to the models. Considering a stationary solution in a frame of reference $\xi = x - c\,t$, moving at constant speed c, the set of partial differential equations reduces to ordinary differential equations which is then recast into an autonomous dynamical system [11]. This dynamical system of finite dimension is solved using a continuation method by Auto07p software [6]. We have focused on solitary-wave solutions to (19) where the hydrodynamics of the film is modeled by the Saint-Venant equations derived by Vila and coworkers

$$\partial_t h = -\partial_x q\,, \tag{22}$$

$$3\mathrm{Re}\partial_t q = -3\mathrm{Re}\partial_x\left(\frac{q^2}{h}+\frac{2}{225}h^5\right) = h - 3\frac{q}{h^2} + \mathrm{We}\partial_{xxx}h \tag{23}$$

Equation (20) has been shown to be limited to low Peclet values as its solutions present nonphysical values of the free-surface temperature, i.e. θ out of the admissible interval [0,1].

We present therefore in figure 3 the evolution of the minimum of θ as a function of the Reynolds number Re. The film is vertical ($\beta = 90°$) and the liquid properties correspond to water ($\mathrm{Ka} = 3000$).

Comparisons to the solutions to the Fourier equation (2d) show that (19) achieves a much better agreement to the reference than the former averaged energy equation (20). Aberrant values of θ are almost unobserved with the new formulation. Yet, a close examination of the distribution of θ (figure 4) under a wave shows that the model (19) overestimates the variations of temperature under the wave. The model also fails to reproduce the jump of free-surface temperature at the front of the wave which is

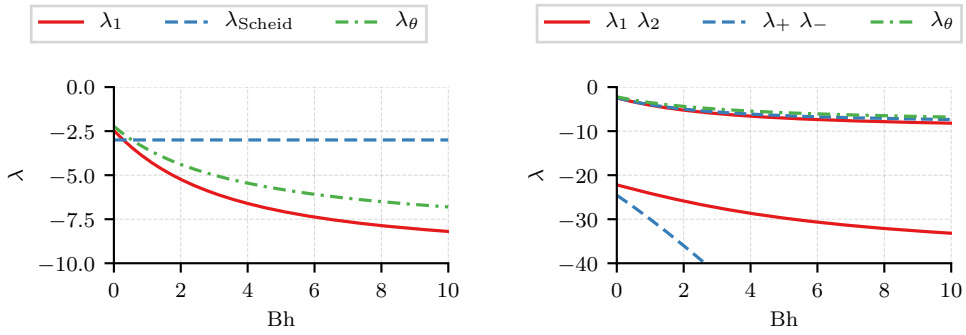

(a) Comparison of the relaxation coefficients in (19) and (20) to the largest eigenvalue λ_1 solution to (7b)

(b) Comparison of the eigenvalues (29) of matrix C (28) to the two first solutions to (7)

Figure 2

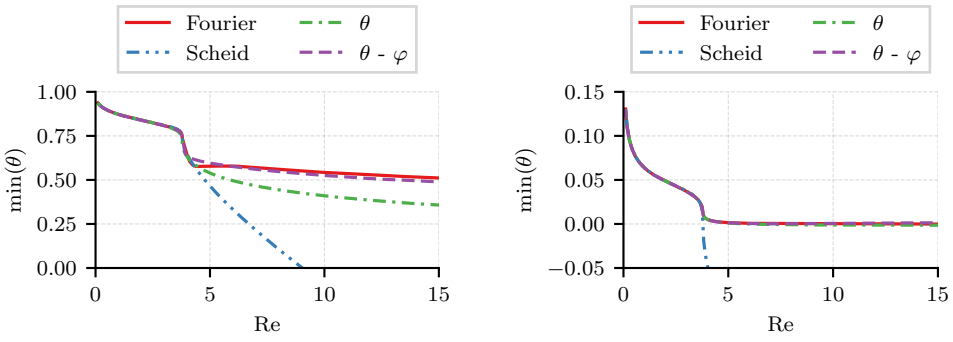

Figure 3: Minimum of the free surface temperature θ under a solitary wave as function of the Reynolds number for a vertical water film ($\beta = 90°$ and Ka = 3000). Left: Pr = 30 and Bi = 0.1 ; right: Pr = 7 and Bi = 10

promoted by the presence of a roll in the wave crest. This rapid variation signals the development of a thermal boundary layer in the vicinity of a hyperbolic stagnation point at the front of the crest (at $h \approx 2.6$ for the discussed solitary wave). The onset of a thermal boundary layer cannot be captured by (20) as θ tends to be a function of h in that case whenever the Peclet number $\mathrm{Pr}\,\mathrm{Re}$ is large as observed in figure 3.

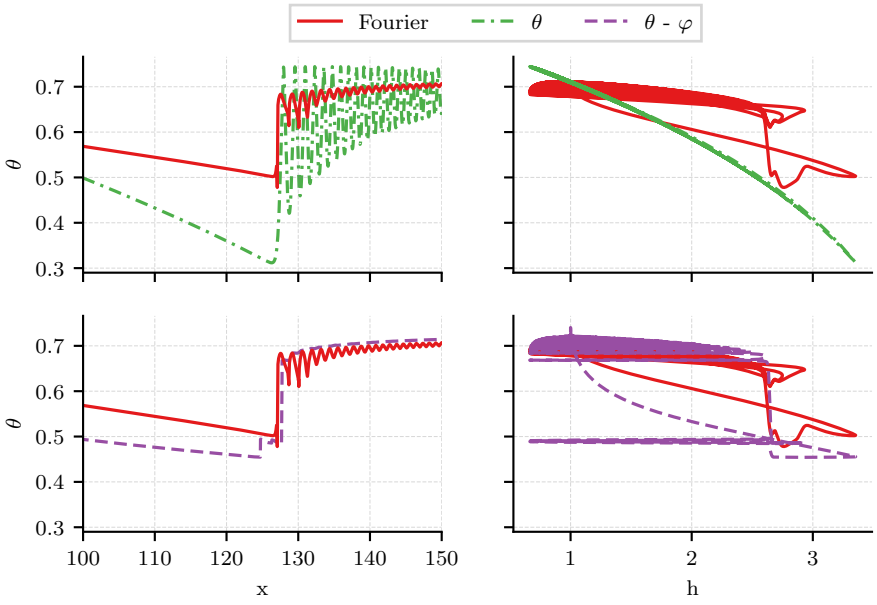

Figure 4: Distribution of the free surface temperature θ under a solitary wave as a function of x (left) and the fluid thickness h (right) for a vertical water film ($\beta = 90°$, Ka $= 3000$, Re $= 33$, Pr $= 30$ and Bi $= 0.1$).

Overcoming these limitations demands to enrich the modeling. We can do so by selecting another variable which reflects the complexity of the temperature field in the vicinity of the free surface. We thus introduce $\varphi = h^2 \partial_{yy} T(y = h)$ such that φ has the dimension of a temperature. Notice that the first derivative $\partial_y T(y = h)$ being involved in the heat balance at the free surface (2h), this variable is equivalent to θ.

We then introduce a more complete ansatz

$$T^{(0)} = [\theta - \theta_0(h)]\hat{v}_1(\bar{y}) + \varphi \hat{v}_2(\bar{y}) \tag{24}$$

where

$$\hat{v}_2 \quad = \quad \frac{1}{2}\bar{y}\,(1-\bar{y})^2 \tag{25}$$

is another linear combination of $\tilde{v}_1$ and $\tilde{v}_2$ verifying $\hat{v}_2'(0) = 1$ and $\hat{v}_2(1) = 0$. The decomposition (24) is made unique by adding

$$\partial_{yy} T^{(1)}|_{y=h} = 0\,. \tag{26}$$

to the gauge condition (17).

Solving (18) then provides an expression of the correction $T^{(1)}$ that is consistent with the ansatz (24) and the long-wave expansion up to first-order for the convective terms and second-order for the diffusion ones.The gauge conditions (26) and (17) then yields coupled evolution equations for the variables θ and φ, namely

$$3\,\mathrm{Pr}\,\mathrm{Re}(\partial_t + u|_{y=h}\partial_x)\theta = \frac{\varphi}{h^2} + 2\mathrm{Bi}\partial_x h\partial_x\theta + \frac{\varphi}{h^2}(\partial_x h)^2 + \mathrm{Bi}\theta\partial_{xx}h + \partial_{xx}\theta \tag{27a}$$

with $u|_{y=h} = \frac{3}{2}q/h$, and

$$\begin{aligned} 3\,\mathrm{Pr}\,\mathrm{Re}\partial_t\varphi \quad = \quad & -3\,\mathrm{Pr}\,\mathrm{Re}\left(\frac{15}{14}\frac{q}{h}\partial_x\varphi + E_\varphi\frac{q}{h}\partial_x\theta + F_\varphi\frac{\partial_x q}{h} + G_\varphi\frac{q\theta}{h^2}\partial_x h\right) \\ & + \frac{1}{h^2}\left\{-60(1+\mathrm{Bi}h)(\theta-\theta_0(h)) - (27+7\mathrm{Bi}h)\varphi\right\} \\ & + J_\varphi\frac{(\partial_x h)^2}{h^2} + \frac{4}{h}\partial_x h\partial_x\varphi + L_\varphi\frac{\partial_x h\partial_x\theta}{h} + \partial_{xx}\varphi \end{aligned} \tag{27b}$$

referred hereinafter as the θ - φ model, with

$$\begin{aligned} E_\varphi \quad &= \quad -\frac{3(25+11\mathrm{Bi}h)}{14}\,, \qquad F_\varphi = -\frac{66+9\varphi+6(38\mathrm{Bi}h-11)\theta}{28}\,, \qquad G_\varphi = \frac{57}{7}\mathrm{Bi}h\,, \\ J_\varphi \quad &= \quad 6-(25+7\mathrm{Bi}h)\varphi+6(2\mathrm{Bi}h-1)\theta\,, \qquad L_\varphi = 48-12\mathrm{Bi}h-14(\mathrm{Bi}h)^2\,. \end{aligned} \tag{27c}$$

The evolution equation (27a) is the trace of the Fourier equation taken at the interface. As a consequence, it is exact and independent of the choice of the polynomials $\hat{v}_1$ and $\hat{v}_2$.

By construction, model (27) is consistent at order ε. The matrix

$$C = \begin{bmatrix} 0 & 1 \\ -60\,(1+\mathrm{Bi}\,h) & -(27+7\,\mathrm{Bi}\,h) \end{bmatrix} \tag{28}$$

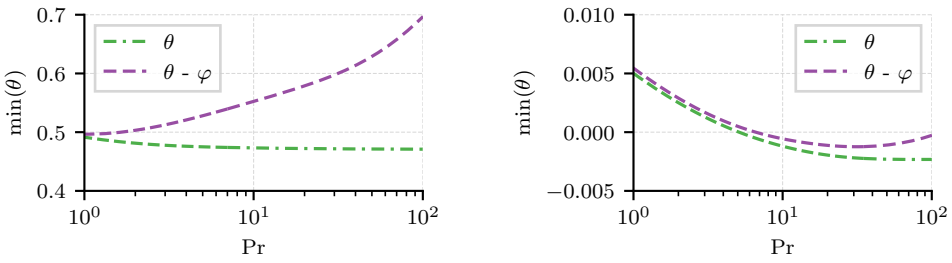

(a) B = 0.1 (b) B = 10

Figure 5: Minimum value of a θ under a solitary wave as function of the Prandtl number.

has eigenvalues

$$\lambda_{\pm} = \frac{1}{2}\left(-27 - 7\mathrm{Bi}h \pm \sqrt{489 + 138\mathrm{Bi}h + 49(\mathrm{Bi}h)^2}\right) \tag{29}$$

We compare (29) to the two first eigenvalues (7) and to the relaxation coefficient (21) in figure 2b. λ_+ is a good approximation to λ_1 whereas λ_- is a poorer one to λ_2. Nevertheless, $\lambda_+ \approx \lambda_1$ shall guarantee that the diffusive relaxation to the linear temperature distribution is correctly captured by the model.

Figure 5 compares the minimum values of the free surface temperature obtained with the one-variable and two-variable model for two Biot number. A minor improvement is observed using two variable for a high Biot number instead of the one-variable model. For both models, $\min(\theta)$ presents nonphysical negative values. The two-variable model remain closer to 0 than the θ model. For both models, this nonphysical behavior is limited compared to previous attempts.

Figure 4 has been completed with the results of the θ - φ model (27). A very noticeable improvement over the θ model (19) can be observed as the sharp variation of the free surface temperature at the hyperbolic stagnation point in the wave is precisely captured by the θ - φ model. This agreement has been obtained over a wide range of B and Pr number.

Figure 6 presents a comparison in the very demanding case of large values of Pr and B numbers where the agreement to the Fourier solution is the least convincing. Yet, the solution to the θ model agrees again well with the Fourier solution in the wave tail, where the film is close to the Nusselt solution (a flat film), but has some trouble to remain

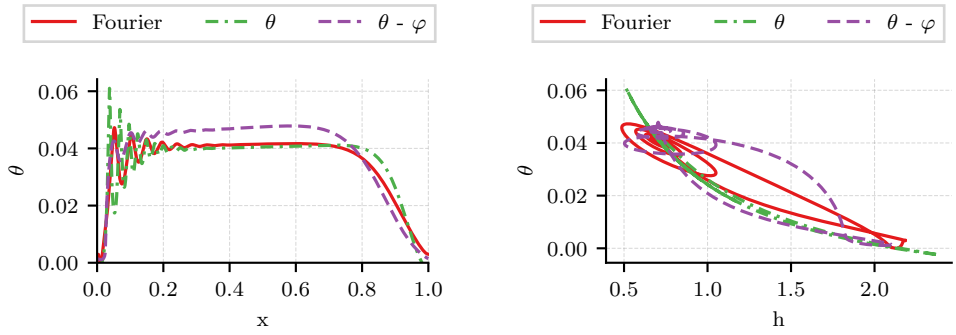

(a) free surface temperature θ according to x (b) free surface temperature θ according to h

Figure 6: Film of water on a vertical wall at $Re = 15$, Bi $= 10$, Pr $= 100$ and $f = 8$ Hz.

accurate as the shape of the wave becomes more complex. It is especially obvious when θ is plotted according to h (fig. 6b). Adding a second variable, more of the temperature surface distribution complexity is captured, $\theta(x)$ mimicking well the reference solution. The simplest model is still advantageous : it shows a good accuracy to capture the averaged properties along the wave.

This is confirmed by the results displayed in figure 7, which presents the global Nusselt number for traveling-wave solutions (computed as the average of the flux at the free surface rescaled by its value for a flat film) according to the wave frequency. The flux being averaged, the θ - φ model main advantage (the ability to represent the complexity of the heat transfer in a more complex hydrodynamic regime) recedes, and the θ model performs somewhat better, especially for high Prandtl number. However both models capture accurately the global heat flux through wave in the thermally developed regime. This is particularly true dealing with water (Pr $= 7$). Departures from the predictions of the Fourier equation can be observed at high values of Prandtl number. Yet, both models provide reasonable answers even at Pr $= 100$.

To conclude, the two models (19 and 27) have different advantages. The first one is robust, and can lead to a better global accuracy. It also uses only one variable to parametrize the thermal transfer, leading to cheaper resolution cost. The latter is able to represent more complex behaviors at a cost of a somewhat lower robustness (and

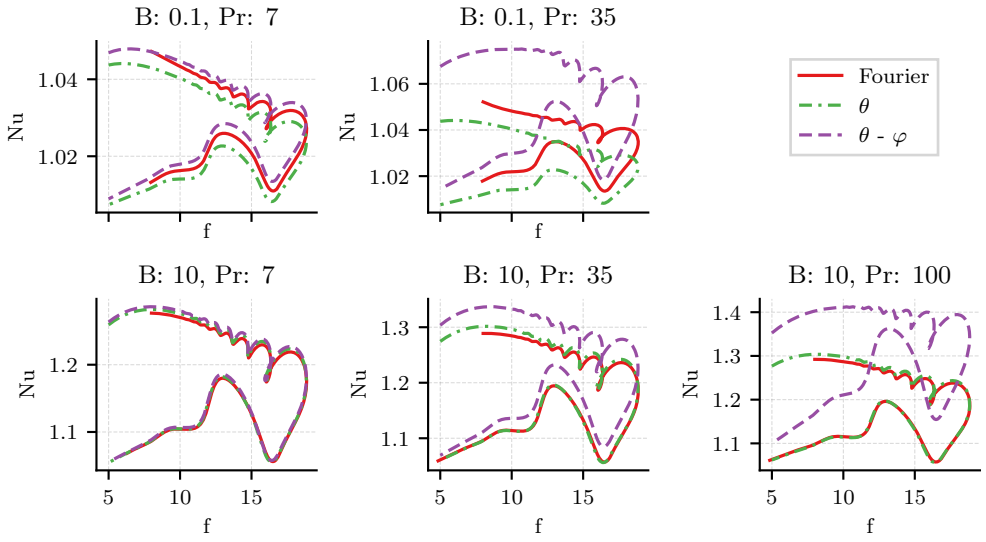

Figure 7: Film of water on a vertical wall at $Re = 15$. The graphs show the global Nusselt number (average of the flux at the free surface rescaled by its value for a flat film). Left Bi = 0.1, right Bi = 10. Top Pr = 7, first row Pr = 35, last row Pr = 100.

global accuracy) and a higher computational cost (which is still far less expansive than solving the full Fourier equation). According to the goal of the study, one or the other may be used.

3. Time dependent simulations

The proposed formulations for the averaged heat balance have been validated by means of computations of the traveling-wave solutions, which implies a thermally and hydrodynamically developed regime. However describing accurately the entrance region of a film flow developing on a plate is crucial for the optimization of a plate exchanger. Therefore, we turn to time-dependent simulations of heat transfer across a 2D liquid falling film. These simulations have been performed using the Saint-Venant hydrody-

namic formulation, proposed by Ruyer-Quil and Manneville [19], which reads as

$$\begin{cases} \partial_t h = -\partial_x q \\ 3\mathrm{Re}\partial_t q = \frac{5\,h}{6} - \frac{5\,q}{2\,h^2} \\ \qquad +\frac{3}{7}\mathrm{Re}\left(9\partial_x h\frac{q}{h} - 17\partial_x q\right)\frac{q}{h} - \frac{5}{6}Ct\,\partial_x h + \frac{5}{6}\mathrm{We}\,h\,\partial_{xxx}h \\ \qquad +\frac{4\,q}{h^2}\partial_x h^2 - \frac{9}{2\,h}\partial_x h\partial_x q - \frac{6\,q}{h}\partial_{xx}h + \frac{9}{2}\partial_{xx}q\,. \end{cases} \tag{30}$$

The reason of this choice is the model's capacity (30) to adequately capture the nonlinear wavy regime of liquid falling films at low to moderate values of the Reynolds number, as demonstrated by comparisons to direct numerical simulation (DNS) (see for instance Ruyer-Quil et al. [21]). In the section 1, the hydrodynamic model has been chosen with a view to making a comparison with the previous study by Chhay et al. [5]. The hydrodynamic parameters are $\mathrm{Re} = 15$, $Ct = 0$ and $\mathrm{We} = 266$ in each case. They correspond to a water film flowing on a vertical plate. This relatively low value of the Reynolds number ensures that the hydrodynamics of the film is adequately captured by the model.

In parallel to the models of heat transfers, we also solved the basic Fourier equation (2d) to provide means of validations. To solve the Fourier equation, a change of coordinates has been performed with $\bar{y} = y/h \in [0, 1]$ instead of $y \in [0, h]$. As a result, the numerical domain is a fixed rectangle $x \in [0, L]$, $\bar{y} \in [0, 1]$, removing the need of a moving mesh.

3.1. Application case example

As an introduction to comparisons between models and their validation with respect to the Fourier basic equation, a typical case is presented here. It corresponds to a water falling film flowing on a vertical plate with an oscillation of its inlet fluid height, periodic in time. We chose a moderate Reynolds number and a low Biot number (as seen in heat exchangers). The parameter set is the following: $Ct = 0$, $\mathrm{Re} = 15$, $\mathrm{We} = 266$, $\mathrm{Pe} = 105$, $\mathrm{B} = 0.1$. The plate is maintained at a hot constant temperature, whereas the fluid flows in contact to a cold atmosphere.

As we can see in the figure 8a, the inlet oscillations grow quickly, leading to a regular saturated wavetrain. These waves consist in one main hump preceded by capillary waves.

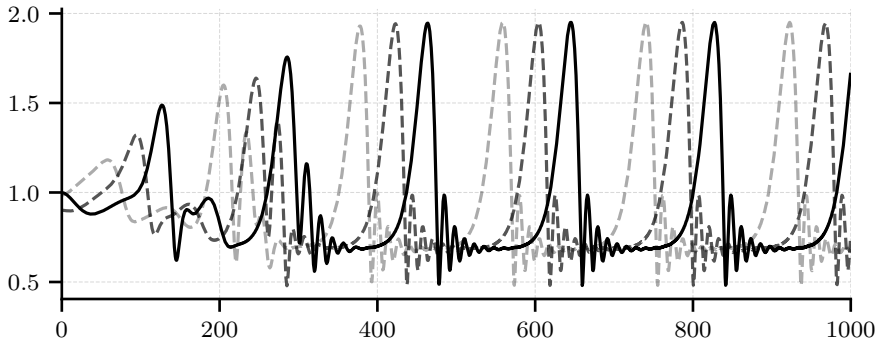

(a) Film height for three successive snapshots.

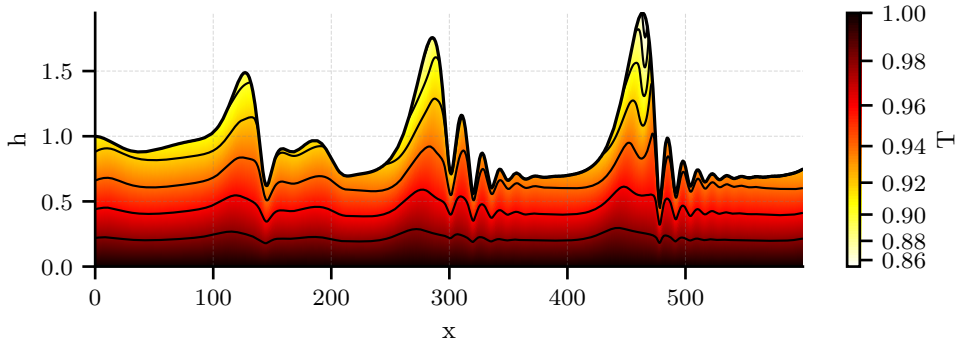

(b) Snapshot of the fluid temperature.

Figure 8: Example study, water flowing over a vertical plate. $Ct = 0$, Re = 15, We = 266, Pe = 105, B = 0.1. Temperature field computed solving the Fourier equation.

These capillary waves are close to each other and have a smaller amplitude than the main hump. Without inlet noise, these waves are evenly spaced and stable in time. Figure 8b shows the temperature field across the film. With moderate-to-high Peclet numbers, we can notice convective effects at the top of the main crest where the cold fluid mixes near the interface mixes slightly with the fluid in the bulk region of the film.

3.2. Comparison between models

Simulations have been first run for a low Peclet number, in order to check the coherence with the Fourier equation. In the low Peclet limit assumption, where the long-wave expansion holds, the temperature fields predicted by the model should agree with the

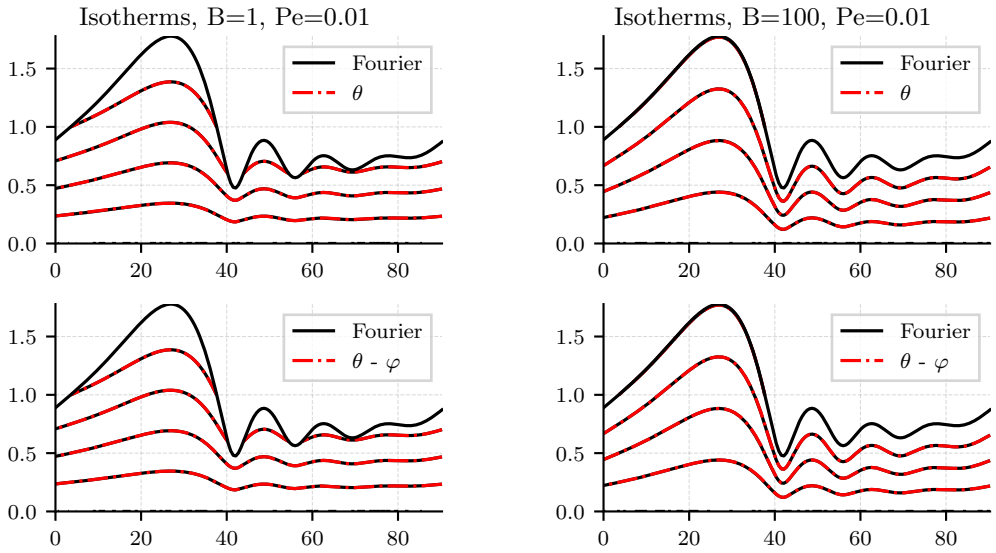

Figure 9: Comparison between the reference case and the different models at low Peclet (Pe = 0.01). Left, B = 1 and right, B = 100. From top to bottom, we have the θ model and the θ - φ with polynomial test functions.

reference solution to the Fourier equation. As we can see in figure 9, in the limit case $\mathrm{Pe} \to 0$, the models present the same behavior as the reference Fourier model, for both moderate and high Biot numbers.

As we increase the Peclet number, we still observe a good agreement with the Fourier equation, even if our models are built on a low Peclet hypothesis (cf. figure 10). As stated previously, the θ model is not complex enough to catch the detail of the temperature field (especially in the crest, near the thermal boundary onset) where the θ - φ models are capable to exhibit a similar complexity. Considering the isotherms close to the wall, the simplest model shows a better agreement with the Fourier equation than the more complex one, where some spurious oscillations can be seen. This is not surprising, as the model is parameterized with only one variable corresponding to the liquid-gas interfacial temperature (where the temperature field presents the greatest complexity). In any case, considering the fact that our derivation assumes order-one values of the Peclet number, the two models show a good agreement with the Fourier equation.

In addition to the periodic-box simulation, simulations of the evolution of the film

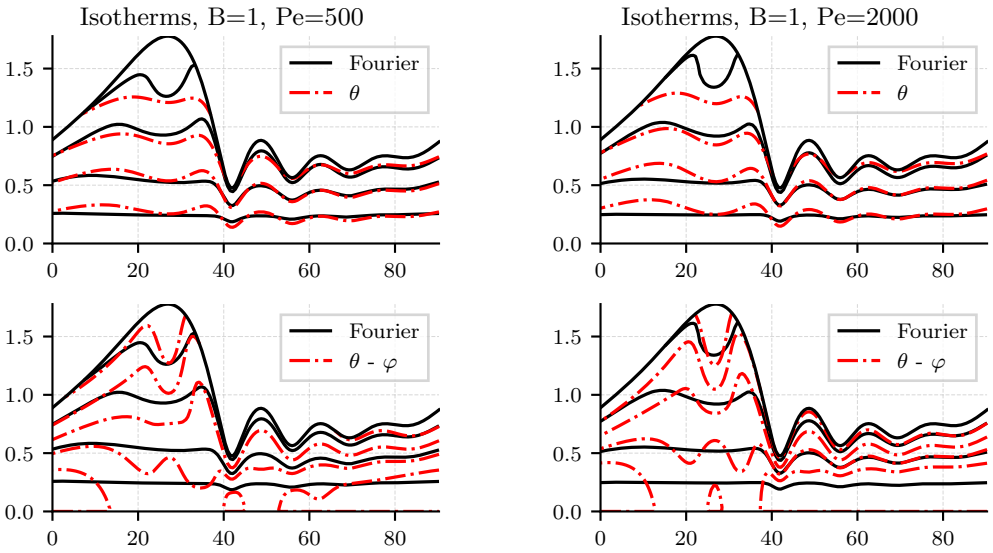

Figure 10: Comparisons between the reference case and the different models at moderate Biot (Bi = 1). Left panel: high Peclet number Pe = 500 (coherent with water thermal properties). Right panel: very high Peclet number Pe = 2000.

in an open large domain, representative of a an element of a plate exchanger, have been performed. This is a critical case, as our previous attempts [4] were unable to capture correctly the onset of the thermally developed regime at the inlet of the flow. The reason for this inaccuracy lies in an incorrect representation of the diffusion relaxation modes discussed in the previous section. The thermal entrance length increases with the Peclet number and can exceed the exchanger length : this is an important factor for the heat exchanger optimization. The same parameters as the periodic-box case have been chosen (Re = 15, $Ct = 0$, We = 266). We modeled a $L = 20$ cm length exchanger plate. A Dirichlet boundary condition has been used at the flow input such as

$$h|_{x=0} = 1 + A\,\sin(2\pi\,t\,f) \quad q|_{x=0} = \frac{1}{3}h^3$$

with the amplitude $A = 0.1$ and the frequency $f = 10$.

The outlet is dealt with a no-flux boundary condition: it yields some numerical errors that are convected outside the domain. We lose a small part of the simulation domain length, and therefore extend the domain to $L = 25$ cm. We then crop a buffer zone to

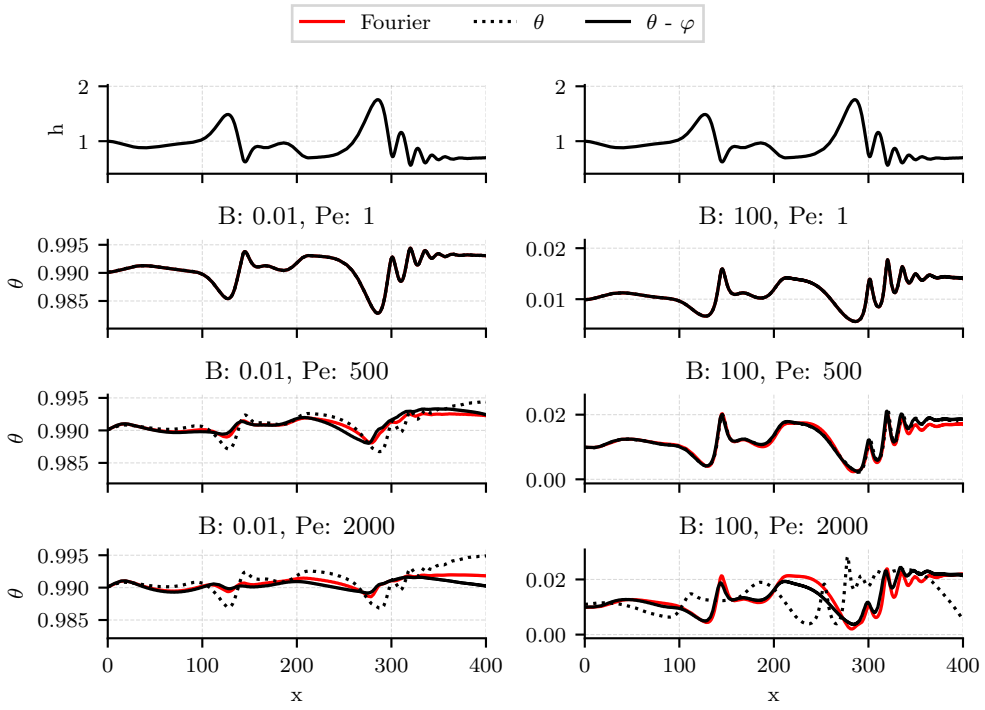

Figure 11: Simulation of a full exchanger plate, first part of the domain. Re = 15, $Ct = 0$, We = 266.

obtain 20 cm of useful length for the simulation.

Figure 11 focuses on the first part of the plate, where the waves are growing. The θ - φ model has the same behavior when the Biot number is low, and shows a slightly better agreement with the Fourier equation than the θ model. Both over-estimate the interfacial temperature.

To check the accuracy of the models for a relaxation process, some simulations have been run for a flat case (without any film perturbation) and a hot film input ($T|_{x=0} = 1$). For the interfacial flux, our two new models (θ and $\theta - \varphi$) have very close behaviors (see figure 12). We are not able to capture the very first part of the relaxation, where the Fourier model goes from no flux at all to local maxima before relaxing. Our model cannot capture such a sharp transition, as a polynomial projection of the temperature field cannot represent a Dirac function. That explains the observed initial flux overshoot. A previous attempt (referred as CFM2015) is unable to capture the relaxation of the

interfacial flux at all.

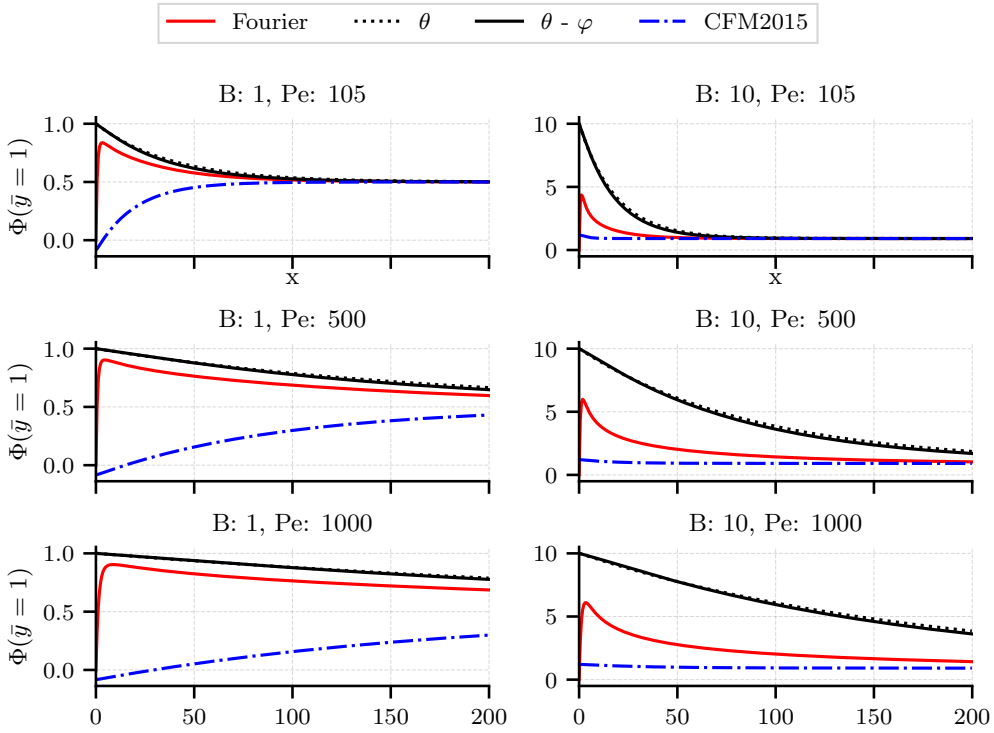

Figure 12: Interfacial heat flux along the flow length, flat film. Re = 15, $Ct = 0$, We = 266.

3.3. Validation - periodic box

A series of simulations have been computed with fixed hydrodynamic parameters, the only varying parameters being the Biot and the Peclet number. The different simulations are compared to the Fourier reference case. The mesh refinement across the film is chosen to depend on the Peclet number as

$$\begin{cases} N_y = 10 & \sqrt{\mathrm{Pe}} < 10 \\ N_y = \sqrt{\mathrm{Pe}} & \text{otherwise.} \end{cases}$$

For very large Peclet numbers, this procedure is not sufficient to guarantee an accurate representation of the temperature field, especially in the vicinity of the thermal boundary layer. However, the obtained accuracy is adequate for the validation of the models.

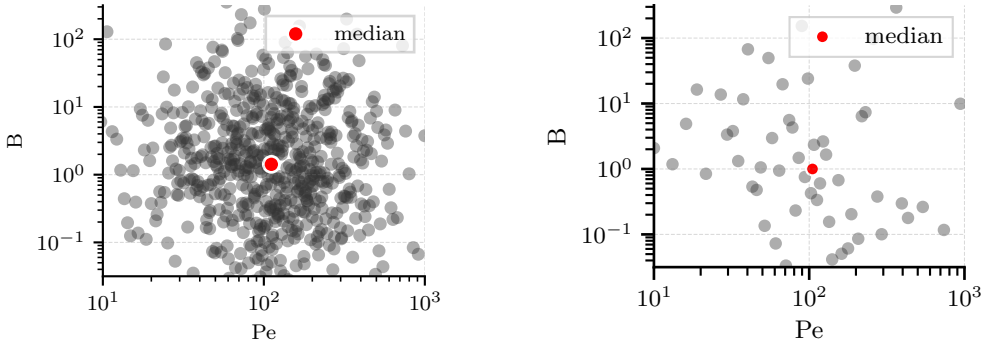

(a) Periodic box study case : 640 samples.

(b) Open flow study case : 64 samples.

Figure 13: Validation sampling: samples chosen with the latin hypercube sampling (LHS) method.

The chosen sampler is a Latin Hypercube Sampler [14] generating samples following a log-normal distribution. The log-normal shapes are chosen in order to fix the median for both varying parameter. The samples are summed up in the figure 13a. The number of samples (640) is large enough to provide a good overview of the behavior of the models according to the two varying parameters.

The two models presented in the previous section are used to simulate a traveling wave in a periodic box of length $L/\bar{h_N} = 90$. The long-time solution of the different models are compared with the reference solution to the Fourier equation. Figure 14 compares the different results. The norm $\mathcal{H}_1$ is defined as

$$\mathcal{L}_{\mathcal{H}_1}(X) = \sqrt{\int X^2 + \frac{\partial X}{\partial x}^2 \, \mathrm{d}x} \,. \tag{31}$$

This norm has been chosen to evaluate both the amplitude and the shape of the heat flux distributions at the interface as predicted by the models. We can observe that the two models exhibit a very good agreement to the reference solutions. For more than half of the physical domain investigated, the error is below a 5% threshold, and never exceed 25%. The θ - φ model presents a wider domain in the parameter space of applicability, defined here by the 5% error threshold. In particular, the range of validity for the Pe number has been extended up to Pe = 100, whatever the value of the B number, which is a significant improvement over the θ model. However, the θ model presents less pronounced maxima of deviation from the Fourier solutions (with a maximal error of 19% instead of 23%),

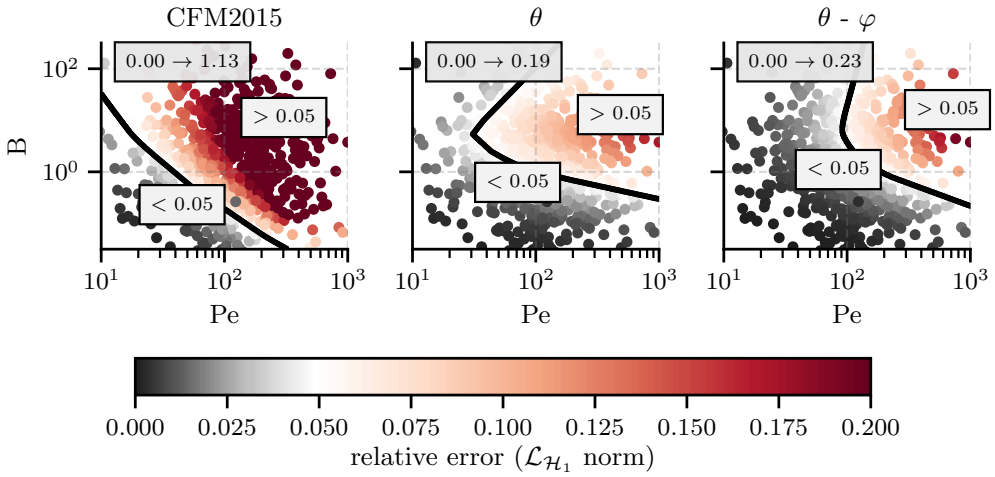

Figure 14: Relative error ($\mathcal{H}_1$ norm) on the wall and interface flux, for the different models. Minimum and maximum error values are displayed at the top left of each plots, and the black border separates the domain where the error is inferior to 5%. This border is determined by training a multi-layered perceptron (MLP) classifier with our data.

but is not able to represent some important phenomena, such as the developing thermal layers near the crest of the waves (as shown in figure 10).

3.4. Validation - full exchanger

The same set of parameters as the periodic-box case has been chosen for the validation case. We have simulated a $L = 20$ cm length exchanger plate. The same boundary conditions as in section 3.2 have been used. A regular forcing at inlet is again enforced with an amplitude equal to $A = 0.1$ and a frequency given by $f = 10$.

Such simulations being expensive in comparison with the periodic-box case, we limit the sample number to 64. The samples can be seen in the figure 13b : the parameter space is well explored and the shape of the log-normal distribution has been chosen so that the median is aligned with our reference case.

As observed in figure 15 (see (31) for the $\mathcal{H}_1$ norm definition), the error of the transient state is smaller than the error for a steady traveling wave, and we have seen that our models relax well to the equilibrium state. The same remarks made for the periodic box stay: the θ model fails to represent the complexity of the temperature field (see figure

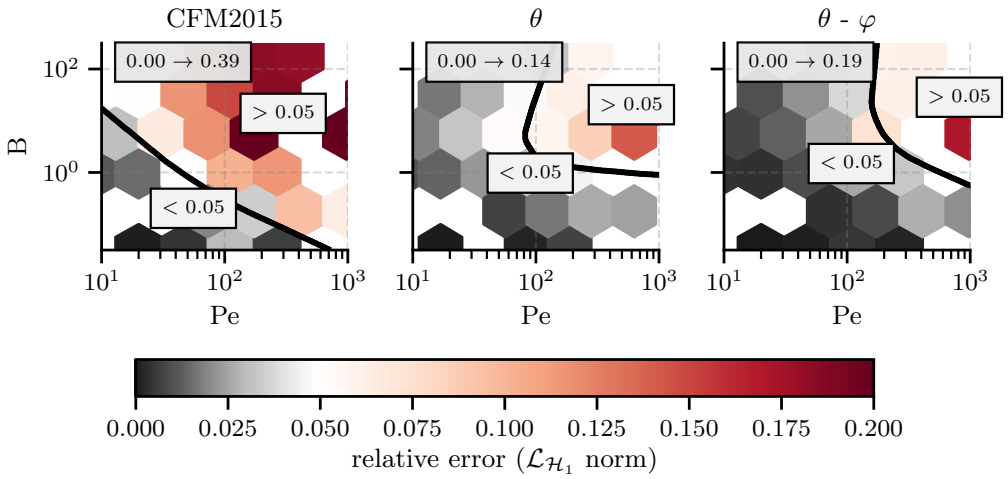

Figure 15: Relative error ($\mathcal{H}_1$ norm) on the wall and interface flux, for the different models. The minimum and maximum error values are displayed at the top left of each plot, and the black border separates the domain where the error is inferior to 5%. This border is determined by training a MLP classifier with our data.

11). Yet, this simple model catches well the interfacial flux with an error below 15%, which is a strong improvement compared to the previous attempts [5, 3].

Conclusion

A new asymptotic model, offered with two variants, has been developed as an alternative to the full resolution of the Fourier equation across a falling film. This leads to a faster resolution at the cost of a reduced domain in the parameter space of applicability (very high Pe numbers are still out of reach). This model overcomes the limitations of previous attempts, which led to acceptable results for moderate Biot and Peclet numbers only, and yielded non-physical behavior outside this range. Moreover, the diffusive relaxation towards the conductive equilibrium in the entrance region of the plate observed with the Fourier equation is now correctly captured. This improves the models accuracy, even outside the entrance regime. It also extends the physical space of applicability (see figure 14, 15), even with only one free variable to represent the temperature distribution (relative error less than 20% for $\mathrm{Pe} \in [10^1, 10^3]$ and $\mathrm{B} \in [10^{-3}, 10^3]$).

The two variants, resp. θ model and θ - φ model, possess different advantages. The simplest one (θ model) is more robust and has a cheaper resolution cost. It is a good candidate for global studies (optimization for example), whereas the second one (θ - φ model) is able to capture more complex thermal transfer behaviors. This complexity has a cost, in terms of robustness and computation especially, at the crest of the waves (due to the extra free variable and evolution equation). That computation cost is still much less expensive than the alternative, i.e. solving the Fourier equation. Hence, this model shows itself to be a good candidate when the comprehension of the phenomena is important but the cost of the Fourier equation cannot be afforded. This cost can be prohibitive when it comes to transfers within a 3D falling film in a spatial domain representative of a realistic plate exchanger. The latter is our next goal, within reach by coupling our model with a computation-efficient shallow-water model developed recently by [2].

This family of models constitutes a new tool which provides a costless evaluation of thermal transfers across a falling film, making costly investigations in terms of number of simulations (optimization, sensitivity analysis, parameterized exploration of the parameter space...) now accessible.

Acknowledgements

The authors acknowledge support by the FRAISE project, grant ANR-16-CE06-0011 of the French National Research Agency (ANR) and by the project Optiwind through Horizon 2020/Clean Sky2 (call H2020-CS2-CFP06-2017-01) with Saint-Gobain.

[1] M. Boutounet. *Modèles asymptotiques pour la dynamique d'un film liquide mince.* PhD thesis, Nov. 2011.

[2] D. Bresch, N. Cellier, F. Couderc, M. Gisclon, P. Noble, G. L. Richard, C. Ruyer-Quil, and J.-P. Vila. Augmented Skew-Symetric System for Shallow-Water System with Surface Tension Allowing Large Gradient of Density. Nov. 2019.

[3] N. Cellier. Thermal falling film modelling, validation and exploration. In *23ème Congrès Français de Mécanique*, Lille, Sept. 2017.

[4] N. Cellier. *Optimisation d'échangeurs à Films Ruisselants.* PhD Thesis, Université Savoie Mont-Blanc, 2018.

[5] M. Chhay, D. Dutykh, M. Gisclon, and C. Ruyer-Quil. New asymptotic heat transfer model in thin liquid films. *Appl. Math. Model.*, 48:844–859, Aug. 2017. ISSN 0307904X. doi: 10/gbk2kg.

[6] E. Doedel, B. Oldeman, et al. AUTO-07p: Continuation and bifurcation software for ordinary differential equations. Concordia University, Montreal, Canada, 2007.

[7] D. P. Frisk and E. J. Davis. The enhancement of heat transfer by waves in stratified gas-liquid flow. *Int. J. Heat Mass Transf.*, 15(8):1537–1552, Aug. 1972. ISSN 00179310. doi: 10/d3d952.

[8] Y. Haroun, D. Legendre, and L. Raynal. Direct numerical simulation of reactive absorption in gas/liquid flow on structured packing using interface capturing method. *Chem. {Engineering} {Science}*, 65(1):351–356, Jan. 2010. ISSN 00092509. doi: 10/dc5pvn.

[9] Y. Haroun, L. Raynal, and D. Legendre. Mass transfer and liquid hold-up determination in structured packing by CFD. *Chem. Eng. Sci.*, 75:342–348, June 2012. ISSN 00092509. doi: 10/f3zm5r.

[10] R. I. Hirshburg and L. W. Florschuetz. Laminar wavy-film flow: Part II, Condensation and evaporation. *J. Heat Transfer*, 104(3):459–464, Aug. 1982. ISSN 00221481. doi: 10/d2xwsd.

[11] S. Kalliadasis, C. Ruyer-Quil, B. Scheid, and M. G. Velarde. *Falling Liquid Films*, volume 176. Springer-Verlag, 2012.

[12] P. Kapitza and S. Kapitza. Wave flow of thin viscous fluid layers. *Zh. Eksp. Teor. Fiz*, 18(3), 1948.

[13] J. D. Killion and S. Garimella. A critical review of models of coupled heat and mass transfer in falling-film absorption. *Int. J. Refrig.*, 24(8):755–797, Dec. 2001. ISSN 01407007. doi: 10/fcr7w7.

[14] M. D. McKay, R. J. Beckman, and W. J. Conover. A Comparison of Three Methods for Selecting Values of Input Variables in the Analysis of Output from a Computer Code. *Technometrics*, 21(2): 239, May 1979. ISSN 00401706. doi: 10/bp9p63.

[15] A. Miyara. Numerical analysis on flow dynamics and heat transfer of falling liquid films with interfacial waves. *Heat Mass Transf.*, 35(4):298–306, 1999. ISSN 0947-7411. doi: 10/d2j5nj.

[16] P.-k. Nguyen, V. Bontozoglou, D. Valourgeorgis, N. Pelekasis, A. N. Andritsos, J. Tsamopoulos, S. G. Yiantsios, and D. Papageorgiou. *Computational Study of Liquid Film Flows along Either Flat or Undulated Substrates*. PhD thesis, 2012.

[17] W. Nusselt. Die Oberflachenkondesation des Wasserdamffes. *Zetrschr. Ver. Deutch. Ing.*, 60:541–546, 1916.

[18] A. J. Roberts. *Model Emergent Dynamics in Complex Systems*. SIAM, 2014. ISBN 1-61197-355-4 978-1-61197-355-6.

[19] C. Ruyer-Quil and P. Manneville. Improved modeling of flows down inclined planes. *Eur. Phys. J. B*, 15(2):357–369, 2000. ISSN 1434-6028. doi: 10/b7p7dk.

[20] C. Ruyer-Quil, B. Scheid, S. Kalliadasis, M. G. Velarde, and R. K. Zeytounian. Thermocapillary long waves in a liquid film flow. Part 1. Low-dimensional formulation. *J. Fluid Mech.*, 538:199–222, 2005. ISSN 0022-1120. doi: 10/d58zwv.

[21] C. Ruyer-Quil, N. Kofman, D. Chasseur, and S. Mergui. Dynamics of falling liquid films. *Eur. Phys. J. E*, 37(4):30, Apr. 2014. ISSN 1292-8941, 1292-895X. doi: 10/ggd9cf.

[22] K. Serifi, N. A. Malamataris, and V. Bontozoglou. Transient flow and heat transfer phenomena in inclined wavy films. *Int. J. Therm. Sci.*, 43(8):761–767, Aug. 2004. ISSN 12900729. doi: 10/ftrc8p.

[23] Y. Y. Trifonov. Stability of the wavy film falling down a vertical plate: The DNS computations and Floquet theory. *Int. J. Multiph. Flow*, 61:73–82, May 2014. ISSN 03019322. doi: 10/f5xs65.

[24] P. N. Yoshimura, T. Nosoko, and T. Nagata. Enhancement of mass transfer into a falling laminar liquid film by two-dimensional surface waves—Some experimental observations and modeling. *Chem. Eng. Sci.*, 51(8):1231–1240, Apr. 1996. ISSN 00092509. doi: 10/fkxgkd.